

Growth of Pure Zinc-Blende GaAs(P) Core–Shell Nanowires with Highly Regular Morphology

Yunyan Zhang,^{*,†,‡} H. Aruni Fonseka,[‡] Martin Aagesen,[§] James A. Gott,[‡] Ana M. Sanchez,^{‡,§} Jiang Wu,^{†,§} Dongyoung Kim,[†] Pamela Jurczak,[†] Suguo Huo,^{||} and Huiyun Liu[†]

[†]Department of Electronic and Electrical Engineering, University College, London WC1E 7JE, United Kingdom

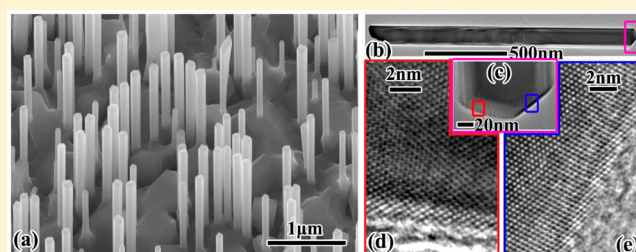
[‡]Department of Physics, University of Warwick, Coventry CV4 7AL, United Kingdom

[§]Center for Quantum Devices, Niels Bohr Institute, University of Copenhagen, Universitetsparken 5, 2100 Copenhagen, Denmark

^{||}London Centre for Nanotechnology, University College, London WC1H 0AH, United Kingdom

ABSTRACT: The growth of self-catalyzed core–shell nanowires (NWs) is investigated systematically using GaAs(P) NWs. The defects in the core NW are found to be detrimental for the shell growth. These defects are effectively eliminated by introducing beryllium (Be) doping during the NW core growth and hence forming Be–Ga alloy droplets that can effectively suppress the WZ nucleation and facilitate the droplet consumption. Shells with pure zinc-blende crystal quality and highly regular morphology are successfully grown on the defect-free NW cores and demonstrated an enhancement of one order of magnitude for room-temperature emission compared to that of the defective shells. These results provide useful information on guiding the growth of high-quality shell, which can greatly enhance the NW device performance.

KEYWORDS: Nanowire, self-catalyzed, shell, beryllium doping, pure zinc-blende



Semiconductor nanowires (NWs) have considerable advantages over conventional planar semiconductors, such as efficient strain relaxation, reduced materials consumption, high aspect ratio, waveguiding ability, and enhanced light-trapping properties.^{1–6} These unique properties offer NWs enormous versatility as novel nanoscale building blocks for the next generation of semiconductor devices.^{17,18} Now, they have demonstrated the applications in areas, such as photovoltaics, light emitters, electron transistors, chemical, biological sensors, and so on.^{7–14} Shell growth is a fundamental way to construct lateral homo- and heterojunctions. It could form advanced structures with novel functionality, i.e., surface passivation layers, quantum wells, p–i–n junctions, and tunnel junctions.^{15,16,19} To make good use of these NW core–shell structures and realize device functionalities, controlled and reproducible shell growth is essential. However, the NW shell growth is significantly different from thin film growth due to the former's inherent structural characteristics, such as cylindrical shape, high aspect ratio, and nanoscale diameter.^{20,21}

For the widely used vapor–liquid–solid (VLS)-grown NWs, the shell growth is even more complicated due to the presence of the liquid catalytic droplet that catalyzes the core growth.²²

Studies on the shell growth on droplet-catalyzed NWs have been heavily reported throughout the past decade. However, a significant proportion of the reported work was based on foreign-metal-catalyzed NW cores²³ (e.g., Au). These foreign catalysts not only introduce the risk of contaminating the NW crystal but also cause problems during the shell growth. Due to

the unconsumable nature, those catalysts cannot be removed in situ, and their existence can lead to continued axial growth that competes with the lateral shell growth, which leads to sharp-pencil-like shell morphology.²⁴ The removal of the catalyst requires removal of the wafer from the growth chamber,²⁵ increasing the cost and the risk of contamination. The self-catalyzed growth mode has thus gained significant attention, especially in the III–V NW growth.²⁶ Because the catalyst material is common with one element of the NW crystal (e.g., Ga catalyst for GaAs NWs), this growth mode has the advantage to consume the droplet before the subsequent shell growth and, hence, can avoid the contamination by foreign metals. However, the self- and foreign-catalyzed NWs have different optimal shell growth conditions, which differentiates the characteristics of the resulting shells.^{20,27} In addition, Au catalyzed zincblende (ZB) NWs are commonly observed to consist of {112} facets, while the self-catalyzed NWs are bounded by {110} facets.⁷ Different facets have different surface energies, which can greatly affect the shell growth. Thus, the knowledge obtained from foreign-metal-catalyzed growth cannot be transferred directly to the self-catalyzed technique.

In recent years, significant effort has been devoted to the development of self-catalyzed core–shell structures.^{28–30} However, the self-catalyzed NWs (except antimonide NWs)

Received: May 16, 2017

Revised: June 26, 2017

Published: July 31, 2017

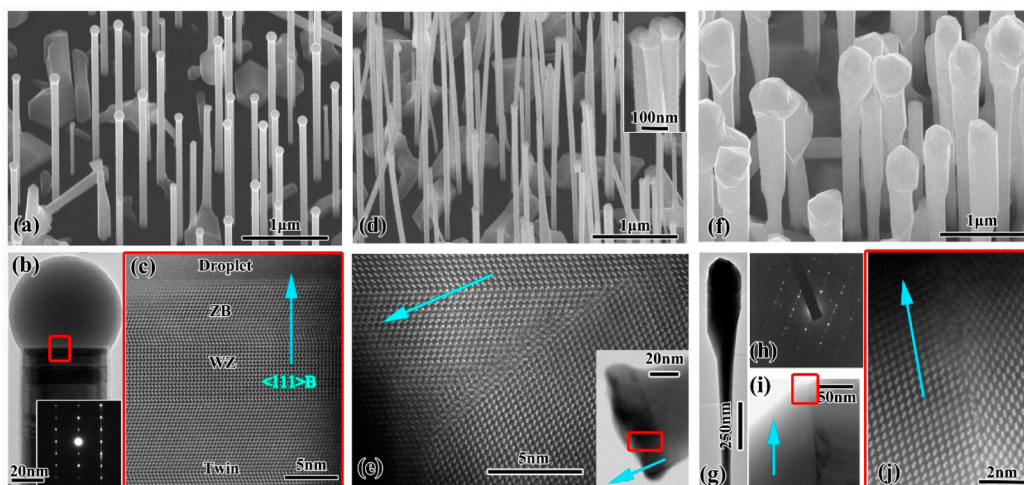


Figure 1. (a) SEM image of GaAs NWs without droplet consumption. (b) TEM image of the NW tip from panel a. The inset is a SAED pattern from the tip region of the NW demonstrating a high density of stacking faults. (c) Atomic-resolution STEM image of the particle–NW interface marked by the red square in panel b. (d) SEM image of droplet consumed GaAs NWs. The inset shows SEM images of the NW tips. (e) Atomic-resolution STEM image of the top region, marked by a red square shown in the inset low-magnification STEM image of the tip of a NW from panel d. (f) SEM image of core–shell GaAs NWs. (g) Low-magnification TEM image of an entire NW from sample in panel f. (h) SAED pattern from the tip region of panel g. (i) Low-magnification TEM image of a growth–grain boundary at the tip of panel g. (j) Atomic-resolution STEM image of the region marked by a red square in panel i. All TEM and STEM images were captured along $\langle 110 \rangle$ zone axis. The blue arrows indicate the NW growth direction of $\langle 111 \rangle$ B.

tend to have stacking faults that are difficult to be eliminated due to the small growth window and the sensitivity of self-catalytic droplets to the growth environment.³¹ The changes in the droplet properties, such as shape, contact angle, and supersaturation, can lead to the formation of defects. For example, the NW tips with improper droplet consumption are commonly observed to have a high density of stacking faults.³² These defects extend to the shell and degrade its crystal quality, as the shell is copying the lattice template from the core. Moreover, the defects can change the NW surface properties, such as the atom arrangements and surface energy, which could also affect the shell growth. More studies regarding how these defects react with the shell growth are needed, especially when the shell needs to be grown under special conditions to realize advanced functions, such as heavily doped tunnel junctions. The detailed theory on how to suppress the formation of these defects is still lacking, and more-detailed studies are needed to grow high-quality shells.

In this paper, the growth of core–shell NWs was studied using the self-catalyzed NWs in the GaAs(P) material system. The defects in the core NWs were found to degrade the shell morphology and crystal quality. By the formation of Be–Ga alloy droplets, defect-free core NWs up to the topmost bilayer have been demonstrated. This leads to the growth of shells with highly regular morphology and pure-ZB crystal quality.

The influence of the defects at the NW tip region on the shell growth was first studied. Figure 1a shows the scanning electron microscope image (SEM) of NWs in which droplet consumption has not taken place. These NWs are uniform in diameter along the length with a round Ga droplet on top (Figure 1b). The interface between Ga droplet and NW crystal is flat. Below the droplet, there is a segment containing ZB–WZ polytypes and stacking faults as can be observed in Figure 1c. After the NW growth, the droplets were consumed during cooled down process by closing the Ga flux and keeping the As open at only 16% of the growth flux. Figure 1d–f corresponds to these NWs whose droplet has been fully consumed. Figure

1d shows that NWs are uniform in diameter along its length, similar to the NWs in Figure 1a. However, their tips are significantly enlarged with sawtooth-like irregular top facets (insets of Figure 1e). Detailed studies show that there are growth and grain boundaries at the enlarged tip (Figure 1e), suggesting that multiple nucleation sites are active during the droplet consumption process. Shell growth was carried out on the NWs shown in Figure 1d, developing a large, irregular lump at the tip of each NW (Figure 1f,g). This region has high density defects, which was confirmed by selected area electron diffraction (SAED) patterns (Figure 1h), recorded in areas containing the growth and grain boundaries shown in Figure 1i,j. The sawtooth like top facets provide more energetically favorable nucleation sites compared with the smoother and lower-surface-energy $\{110\}$ sidewalls, originating these irregular tips.¹⁵ Besides, the tip collects source materials more effectively because the fluxes come from the top, making the tip grow faster.

Results shown in Figure 1 evidence the influence of growth and grain boundaries observed in the NW core on the shell growth. A more detailed analysis of the impact of the defects, mainly stacking faults and multiple twinning observed in the core, on the shell was also carried out. The inset in Figure 2a reveals how the defects in the core NW extend into the shell, i.e., the shell growth follows the core lattice structure. It is found that when Be dopant is introduced during the shell growth onto a defective core, the shell quality can be further degraded. As shown in Figure 2b, when grown with a Be flux that results in a nominal doping concentration of $6 \times 10^{18} \text{ cm}^{-3}$, the resulting NWs have enlarged lumps along the length of the NW. Each lump has a twin plane across its widest diameter (Figure 2c) and is often multiple-twinned (bottom left of panels c and f of Figure 2), i.e., twin planes are extended into other $\{111\}$ planes with at angle of 54.7° relative to the growth plane. If the core has a high density of defects, the surface of the resulting shell is rough (Figure 2d). Nevertheless,

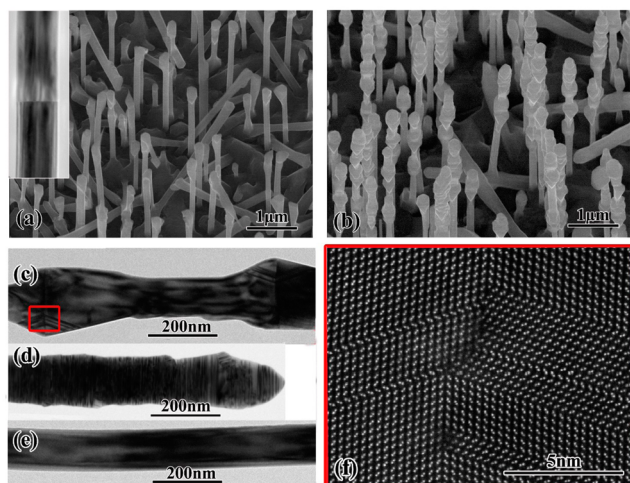


Figure 2. Core-shell GaAsP NWs with a nominal doping concentration of (a) 0 and (b) $6 \times 10^{18} \text{ cm}^{-3}$, respectively, in the shell. The inset in panel a is a low-magnification TEM image of a segment from a NW in panel a. (c–e) Low-magnification TEM image of NW segments from panel b with different stacking fault densities: (c) with single twin planes perpendicular to the growth direction and multiple inclined twins at lumps, (d) with high density of stacking faults perpendicular to the growth direction, and (e) without stacking faults. (f) Atomic-resolution STEM image of the twin plane area marked in the red square of panel c. All TEM images are captured along the $\langle 110 \rangle$ zone axis.

a defect-free core NW results into a smooth shell that is free of lumps (Figure 2e).

Self-catalyzed NWs are bounded by the $\{110\}$ facets, which are expected to have lowest surface energy for self-catalyzed NWs.^{15,33} When there are stacking faults and twin planes, the atom arrangement at the surface changes, exposing new facets with higher surface energy. Nucleation at these sites is thus energetically preferable. Be is known to act as a surfactant that can improve the mobility of Ga adatoms.³⁴ Hence, when the shell is grown with a high concentration of Be dopant, Ga with the enhanced mobility has a greater chance to move to and accumulate at these locations. This results in these areas growing much faster than the defect-free locations and, therefore, forming the lumps. The dislocations, e.g., high-angle grain boundaries, shown in Figure 2f could also result from the same excessively fast nucleation rate.³⁵ These phenomena are similar to a previous report by Zou et al.³⁶ They also observed the formation of big lumps during the shell growth. However, the lumps were formed at defect-free locations. This is because that their NWs were grown by Au-catalyzed mode and are bounded by $\{112\}$ facets with high surface energy. At twin areas, the newly formed facets are lower in surface energy compared with $\{112\}$ facets. Thus, the shell growth rate at defect-free areas is faster.

The above observations clearly demonstrate that the defect at the core can strongly affect the shell growth and crystal quality. A defect-free core is thus essential for high-quality shell growth. To achieve this, Be doping with a nominal concentration of $6.4 \times 10^{18} / \text{cm}^3$ was introduced during the core NW growth. The introduction of Be significantly improves the tip morphology, making it without enlargement or sawtooth top facets. This is in contrast to the results presented in Figure 1d. Figure 3a,b shows NWs with uniform diameter along the length. The tip is quite sharp, suggesting a gradual shrinkage of the droplet.

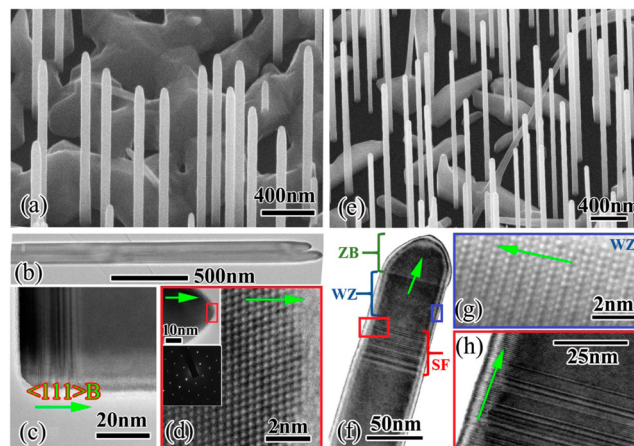


Figure 3. (a) SEM images of droplet-consumed GaAs NWs with nominal Be doping concentrations of $6.4 \times 10^{18} / \text{cm}^3$. (b) Low-magnification TEM image showing two NWs from panel a. (c) Zoomed-in TEM image shows the bottom of a NW shown in panel b revealing defects in that area. (d) High-resolution TEM image at the top of the tip (marked by a red square in its inset). The insets show a low-magnification TEM image and the SAED pattern of the NW tip shown in panel b. (e) SEM images of droplet-consumed GaAs NWs with nominal Be doping concentrations of $8 \times 10^{17} / \text{cm}^3$. (f) Low-magnification TEM image shows the tip of a NW from panel e. (g, h) Higher-magnification TEM images of the areas marked by squares in (f). All TEM images are captured along $\langle 110 \rangle$ zone axis. The green arrows indicate the NW growth direction of $\langle 111 \rangle$ B.

There is no defect-related contrast except at the very bottom of the NW (Figure 3b,c). Additionally, high-resolution images in Figure 3d show that the tip is defect-free up to the topmost bilayer. The presence of Be inside the droplet affects the droplet properties, such as the surface energy and supersaturation, which can make the nucleation environment beneficial for ZB structure. This can be confirmed by the NWs from a comparison sample with a much-lower nominal Be doping concentrations of $8 \times 10^{17} / \text{cm}^3$ (Figure 3e). Due to the small doping flux, the Be concentration inside the Ga droplets is low, and the change of droplet properties is small. As a result, a high density of stacking faults is observed (Figure 3f,g). These results show that the Be can promote the ZB nucleation during the NW growth and facilitate the stacking-fault-free single-crystalline droplet consumption at the end of NW growth.

Shell growth was carried out on defect-free NW cores, optimized as previously described (Figure 3a). Here again, NWs are uniform in diameter along its length (Figure 4a,b)

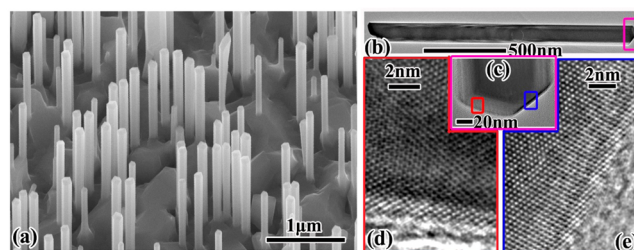


Figure 4. SEM image of core-shell GaAsP NWs. (b) Low-magnification TEM image that shows an entire NW from (a). (c) Low-magnification TEM image shows the tip of panel b. (d, e) High-resolution TEM image of the regions marked by squares in panel c. All TEM images are captured along the $\langle 110 \rangle$ zone axis.

with a tip bounded by well-developed facets (Figure 4c). As shown in Figure 4b, the entire NW does not show any defect-related contrast. This NW is defect free up to the topmost bilayer as shown in Figures 4d,e, which is in good agreement with the core NWs shown in Figure 3. Even for some NWs with defects, there are only one or two single twin planes that can be observed along the entire NW. Large-area statistics show an average of ~ 1.5 single twin defects per NW.

We note here that the morphology of a defect-free core is not critical in controlling the shell morphology. Despite the sharp morphology of the core, the tip of the core-shell NWs shown in Figure 4 can still form well-developed facets. This process is controlled by the surface energy of facets.¹⁵ The facets with higher surface energy grow faster, while the ones with lower surface energy grow slower. This can cause the area shrinkage of the high-growth-rate facets and area expansion of low-growth-rate facets during the shell growth. The entire NW is bounded by the $\{110\}$ facets with low surface energy at the end.

The optical properties of the core-shell NWs with different shell quality were investigated by photoluminescence (PL). The room-temperature PL spectra from NW ensembles of different core-shell quality are shown in Figure 5. Due to the presence

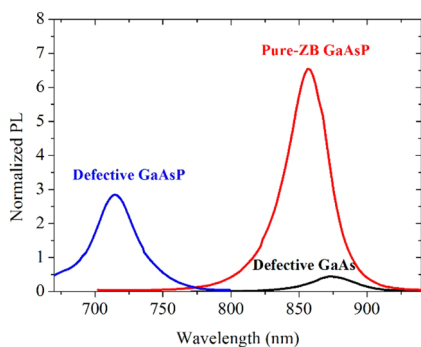


Figure 5. Room-temperature PL spectra obtained from GaAs(P) NWs with good (red, Figure 4 sample) and poor (black, Figure 1f sample; blue, Figure 2a sample) core-shell quality.

of P, the spectra of GaAsP NWs are blue-shifted compared to the spectrum of GaAs NWs. The single peak emission suggests that the core and shell of GaAsP NWs are almost identical in P composition. The peak intensity of GaAsP NWs with good shell quality (red) is enhanced by a factor of 15 and 2.3 compared with that of the defective GaAs (black) and GaAsP (blue) NWs. The enhancement of PL emission from high-quality core-shell NWs is predominantly due to the elimination of the defects that act as nonradiative recombination centers, such as that shown in Figure 1e,j. The doping could also assist the PL emission due to the change of band structure, such as changing surface depletion width and partially filling the surface states.^{37,38} Therefore, doping of core NWs can result in both good core-shell crystal quality and optical properties.

In conclusion, the growth of self-catalyzed core-shell NWs was investigated systematically using MBE grown GaAs and GaAsP NWs. The defects from the core are found to be able to extend into the shell, which degraded the shell crystal quality. These defects can also regionally change the surface properties of NWs, such as creating new nucleation facets with different surface energies. This can lead to the change of the nucleation features around these defective regions and affect the shell uniformity, which has been demonstrated by the Be-doped shell

with kabob-like morphology. Elimination of defects in the core NWs is essential to achieve high-quality shell growth, which can be achieved by introducing Be doping during the growth. The formation of Be-Ga alloy droplets can effectively suppress the WZ nucleation and facilitate the droplet consumption, leading to the phase-pure ZB NWs. Shell with pure-ZB crystal quality and highly regular morphology can be grown on the defect-free core NWs and has demonstrated one-order room-temperature emission enhancement compared to the defective shell. These results provide useful information for constructing the high-quality core-shell NW devices.

Methods. NW Growth. The self-catalyzed GaAs and GaAsP nanowires were grown directly on p-type Si(111) substrates by solid-source III-V molecular beam epitaxy (MBE).^{15,39} GaAs NWs were grown with a Ga beam equivalent pressure, V-to-III flux ratio, substrate temperature, and growth duration of 8.41×10^{-8} Torr, 44, ~ 630 °C, and 1 h, respectively. The GaAs shell was grown with a Ga beam equivalent pressure, V-to-III flux ratio, substrate temperature, and growth duration of 8.41×10^{-8} Torr, 50, ~ 480 °C, and 150 min, respectively. GaAsP NWs were grown with a Ga beam equivalent pressure, V-to-III flux ratio, P/(As + P) flux ratio, substrate temperature, and growth duration of 8.41×10^{-8} Torr, 40, 12%, ~ 640 °C and 1 h, respectively. The GaAsP shell was grown with a Ga beam equivalent pressure, V-to-III flux ratio, P/(As + P) flux ratio, substrate temperature, and growth duration of 8.41×10^{-8} Torr, 50, 30%, ~ 500 °C, and 60 min, respectively. After the NW growth, the droplets were consumed by closing the Ga flux and keeping the As open at only 16% of the growth flux. But if no droplet consumption was performed, Ga, As, and GaAsP were all closed to keep the droplets. The nominal Be doping concentration is characterized in thin film growth with GaAs growth rate of 1 ML/s. The substrate temperature was measured by pyrometer.

Scanning Electron Microscopy. The NW morphology was measured with a Zeiss XB 1540 focused ion beam-scanning electron microscope system.

Transmission Electron Microscopy. Simple scraping of the NWs onto a holey carbon support was used to prepare transmission electron microscopy (TEM) specimens. The TEM measurements were performed on JEOL 2100 and doubly corrected ARM200F microscopes, both operating at 200 kV.

Photoluminescence. The photoluminescence measurement was performed at room temperature using a nanometrics RPM2000 machine with an excitation wavelength of 635 nm and a power density of ~ 500 W/cm².

■ AUTHOR INFORMATION

Corresponding Author

*E-mail: yunyan.zhang.11@ucl.ac.uk.

ORCID

Yunyan Zhang: 0000-0002-2196-7291

Ana M. Sanchez: 0000-0002-8230-6059

Jiang Wu: 0000-0003-0679-6196

Notes

The authors declare no competing financial interest.

■ ACKNOWLEDGMENTS

The authors acknowledge the support of Leverhulme Trust and EPSRC (grant nos. EP/P000916/1 and EP/P000886/1).

REFERENCES

- (1) Dick, K. A. *Prog. Cryst. Growth Charact. Mater.* **2008**, *54*, 138–173.
- (2) Lieber, C. M.; Wang, Z. L. *MRS Bull.* **2007**, *32*, 99–108.
- (3) Zhang, Y.; Wu, J.; Aagesen, M.; Liu, H. *J. Phys. D: Appl. Phys.* **2015**, *48*, 463001.
- (4) Yan, R.; Gargas, D.; Yang, P. *Nat. Photonics* **2009**, *3*, 569–576.
- (5) Dasgupta, N. P.; Sun, J.; Liu, C.; Brittman, S.; Andrews, S. C.; Lim, J.; Gao, H.; Yan, R.; Yang, P. *Adv. Mater.* **2014**, *26*, 2137–2184.
- (6) Yang, P.; Yan, R.; Fardy, M. *Nano Lett.* **2010**, *10*, 1529–1536.
- (7) Joyce, H. J.; Gao, Q.; Tan, H. H.; Jagadish, C.; Kim, Y.; Zou, J.; Smith, L. M.; Jackson, H. E.; Yarrison-Rice, J. M.; Parkinson, P.; Johnston, M. B. *Prog. Quantum Electron.* **2011**, *35* (2), 23.
- (8) Wu, J.; Li, Y.; Kubota, J.; Domen, K.; Aagesen, M.; Ward, T.; Sanchez, A.; Beanland, R.; Zhang, Y.; Tang, M.; Hatch, S.; Seeds, A.; Liu, H. *Nano Lett.* **2014**, *14*, 2013–2018.
- (9) Zhuang, Q. D.; Anyebe, E. A.; Chen, R.; Liu, H.; Sanchez, A. M.; Rajpalke, M. K.; Veal, T. D.; Wang, Z. M.; Huang, Y. Z.; Sun, H. D. *Nano Lett.* **2015**, *15* (2), 1109–1116.
- (10) Arafin, S.; Liu, X.; Mi, Z. *J. Nanophotonics* **2013**, *7* (1), 074599–074599.
- (11) LaPierre, R. R.; Chia, A. C. E.; Gibson, S. J.; Haapamaki, C. M.; Boulanger, J.; Yee, R.; Kuyanov, P.; Zhang, J.; Tajik, N.; Jewell, N.; Rahman, K. M. *Phys. Status Solidi RRL* **2013**, *7* (10), 815–830.
- (12) Wu, J.; Ramsay, A.; Sanchez, A. M.; Zhang, Y.; Kim, D.; Brossard, F. S. F.; Salamo, G. G.; Aagesen, M.; Wang, Z.; Liu, H.; et al. *Nano Lett.* **2016**, *16*, 504.
- (13) Borgström, M. T.; Wallentin, J.; Heurlin, M.; Fält, S.; Wickert, P.; Leene, J.; Magnusson, M. H.; Deppert, K.; Samuelson, L. *IEEE J. Sel. Top. Quantum Electron.* **2011**, *17* (4), 1050–1061.
- (14) Couteau, C.; Larrue, A.; Wilhelm, C.; Soci, C. *Nanophotonics* **2015**, *4* (1), 90–107.
- (15) Zhang, Y.; Sanchez, A. M.; Wu, J.; Aagesen, M.; Holm, J. V.; Beanland, R.; Ward, T.; Liu, H. *Nano Lett.* **2015**, *15*, 3128–3133.
- (16) Parkinson, P.; Joyce, H. J.; Gao, Q.; Tan, H. H.; Zhang, X.; Zou, J.; Jagadish, C.; Herz, L. M.; Johnston, M. B. *Nano Lett.* **2009**, *9* (9), 3349–3353.
- (17) Royo, M.; De Luca, M.; Rurali, R.; Zardo, I. *J. Phys. D: Appl. Phys.* **2017**, *50* (14), 143001.
- (18) Saxena, D.; Jiang, N.; Yuan, X.; Mokkaapati, S.; Guo, Y.; Tan, H. H.; Jagadish, C. *Nano Lett.* **2016**, *16* (8), 5080–5086.
- (19) Holm, J. V.; Jørgensen, H. I.; Krogstrup, P.; Nygård, J.; Liu, H.; Aagesen, M. *Nat. Commun.* **2013**, *4*, 1498.
- (20) Zhang, Y.; Sanchez, A. M.; Sun, Y.; Wu, J.; Aagesen, M.; Huo, S.; Liu, H.; Kim, D.; Jurczak, P.; Xu, X. *Nano Lett.* **2016**, *16* (2), 1237–1243.
- (21) Zhang, Y. Y.; Yao, G. R. *J. Appl. Phys.* **2011**, *110* (9), 093104.
- (22) Wagner, R. S.; Ellis, W. C. *Appl. Phys. Lett.* **1964**, *4*, 89–90.
- (23) Dick, K. A.; Caroff, P. *Nanoscale* **2014**, *6* (6), 3006–3021.
- (24) Mohseni, P. K.; LaPierre, R. R. *Nanotechnology* **2009**, *20*, 025610.
- (25) Heurlin, M.; Hultin, O.; Storm, K.; Lindgren, D.; Borgström, M. T.; Samuelson, L. *Nano Lett.* **2014**, *14* (2), 749–753.
- (26) Fontcuberta i Morral, A.; Colombo, C.; Abstreiter, G.; Arbiol, J.; Morante, J. R. *Appl. Phys. Lett.* **2008**, *92* (6), 063112.
- (27) Joyce, H. J.; Gao, Q.; Tan, H. H.; Jagadish, C.; Kim, Y.; Zhang, X.; Guo, Y.; Zou, J. *Nano Lett.* **2007**, *7* (4), 921–926.
- (28) Dobrovolsky, A.; Sukritanon, S.; Kuang, Y.; Tu, C. W.; Chen, W. M.; Buyanova, I. A. *Small* **2014**, *10* (21), 4403–4408.
- (29) Rudolph, D.; Funk, S.; Döblinger, M.; Morkötter, S.; Hertenberger, S.; Schweickert, L.; Becker, J.; Matich, S.; Bichler, M.; Spirkoska, D.; Zardo, I.; Finley, J. J.; Abstreiter, G.; Koblmüller, G. *Nano Lett.* **2013**, *13*, 1522.
- (30) Mayer, B.; Rudolph, D.; Schnell, J.; Morkötter, S.; Winnerl, J.; Treu, J.; Müller, K.; Bracher, G.; Abstreiter, G.; Koblmüller, G.; Finley, J. J. *Nat. Commun.* **2013**, *4*, 2931.
- (31) Zhang, Y.; Aagesen, M.; Holm, J. V.; Jørgensen, H. I.; Wu, J.; Liu, H. *Nano Lett.* **2013**, *13*, 3897–3902.
- (32) Heon Kim, Y.; Woo Park, D.; Jun Lee, S. *Appl. Phys. Lett.* **2012**, *100* (3), 033117.
- (33) Dick, K. A.; Caroff, P.; Bolinsson, J.; Messing, M. E.; Johansson, J.; Deppert, K.; Wallenberg, L. R.; Samuelson, L. *Semicond. Sci. Technol.* **2010**, *25*, 024009.
- (34) Gutiérrez, M.; Araujo, D.; Jurczak, P.; Wu, J.; Liu, H. *Appl. Phys. Lett.* **2017**, *110* (9), 092103.
- (35) Sanchez, A. M.; Zhang, Y.; Tait, E. W.; Hine, N. D.; Liu, H.; Beanland, R. *Nano Lett.* **2017**, *17* (4), 2454–2459.
- (36) Zou, J.; Paladugu, M.; Wang, H.; Auchterlonie, G. J.; Guo, Y.; Kim, Y.; Gao, Q.; Joyce, H. J.; Tan, H. H.; Jagadish, C. *Small* **2007**, *3*, 389–393.
- (37) Demichel, O.; Heiss, M.; Bleuse, J.; Mariette, H.; Fontcuberta i Morral, A. *Appl. Phys. Lett.* **2010**, *97*, 201907.
- (38) Chia, A. C. E.; LaPierre, R. R. *J. Appl. Phys.* **2012**, *112*, 063705.
- (39) Zhang, Y.; Wu, J.; Aagesen, M.; Holm, J.; Hatch, S.; Tang, M.; Huo, S.; Liu, H. *Nano Lett.* **2014**, *14*, 4542–4547.